

RESEARCH

Open Access



# Transcriptomics and proteomics reveal associations between myometrium and intrauterine adhesions

Xiaotong Xu<sup>1,2†</sup>, Kaixuan Guo<sup>1,2†</sup>, Peng Zhao<sup>3</sup>, Xuemei Zhang<sup>4</sup>, Pan Zhao<sup>5</sup>, Xianghang Sun<sup>1,2</sup>, Mingle Zhang<sup>1,2</sup>, Yanpeng Tian<sup>6</sup>, Li Fen<sup>7</sup>, Jiahua Zheng<sup>1,2\*</sup> and Xianghua Huang<sup>1,2\*</sup>

## Abstract

**Background** Intrauterine adhesions (IUAs) is a gynecological condition with a poor therapeutic prognosis, that severely threatens the fertility and the reproductive physiology and psychological health of women. Our previous research on the use of umbilical cord mesenchymal stem cells (HUCMSCs) for treating IUAs revealed that CM-Dil-labelled HUCMSCs were barely distributed in the endometrial epithelium. Instead, these cells were predominantly found in the myometrium, with no statistically significant difference in distribution compared to the endometrial stromal cells. Therefore, we aimed to explore the associations between the myometrium and IUAs.

**Methods** Eight patients with moderate and 5 severe lesional IUAs were included in the experimental group. The control group included 7 patients whose inner and outer myometrium were normal. We used H&E, Masson's trichrome and immunohistochemical staining to obtain the pathological features of the tissues. Transcriptomic and proteomic analyses were conducted to identify differentially expressed genes, proteins and enrichment pathways.

**Results** Both IUAs lesion tissues expressed the smooth muscle markers  $\alpha$ -SMA and H-caldesmon, and there was no significant difference between severe IUAs tissue and normal myometrium ( $p > 0.05$ ). Transcriptomic and proteomic data revealed that genes and proteins involved in cell mitosis, such as KIF14, KIF4A, and CIT, were downregulated in both IUAs lesion tissues compared with the inner myometrium ( $p < 0.05$ ). Additionally, some genes or proteins that participate in activating the complement-coagulation cascade system and extracellular matrix (ECM) degradation also significantly differed ( $p < 0.05$ ).

**Conclusions** Transcriptomic and proteomic data revealed a correlation between endometrial injury and the myometrium. These findings preliminarily revealed that the myometrium possibly contributes to the aetiology and progression of IUAs through dual mechanisms. On the one hand, the myometrium inhibits endometrial regeneration by suppressing the cell mitogenic pathway. On the other hand, it promotes fibrosis by activating the complement-coagulation cascade system and inhibiting the ECM degradation pathway. These new findings increase our understanding of the pathogenesis of IUAs and potentially contribute to the application of precision clinical treatment for IUAs.

**Keywords** Intrauterine adhesions, Intrauterine myometrium, Transcriptomics, Proteomics

<sup>†</sup>Xiaotong Xu and Kaixuan Guo contributed equally to this work and share first authorship.

\*Correspondence:

Jiahua Zheng  
xiaodelan17@163.com  
Xianghua Huang  
huangxh2022@hebm.edu.cn

Full list of author information is available at the end of the article



## Introduction

Intrauterine adhesions (IUAs), also known as Asherman's syndrome, is a common gynecological condition with a poor therapeutic prognosis, that threatens fertility and severely affects the reproductive physiology and psychological health of women. IUAs occurs due to the adhesion between the uterine muscle walls following damage to the basal layer of the endometrium. The repair process involves three brief and overlapping phases: the inflammatory phase, the tissue formation phase, and the tissue remodelling phase [1]. The regeneration of the endometrium is mostly incomplete and its function is compromised, resulting in the formation of scars. The aetiology and pathogenesis of IUAs are not fully understood. The active fibroblast proliferation theory and the neural reflex theory are currently the most accepted [2]. The incidence of IUAs remains high and is increasing annually with increasing surgeries in the uterus. According to the literature, the incidence of IUAs following abortion, postpartum intrauterine procedures and submucosal myomectomy is as high as 19% to 45.5%, making this condition a major cause of reduced menstrual flow and secondary infertility [3, 4]. Additionally, in the context of IUAs, pregnancies are associated with an increased risk of adverse obstetric outcomes, such as ectopic pregnancies, recurrent miscarriages, preterm labour, and placental abnormalities [5]. Transcervical resection of adhesions (TCRA) is acknowledged as the primary therapy for IUAs, but the readhesion rate after TCRA can reach 60% [6]. Hyaluronic acid (HA) gel was identified as a Level A evidence-based mechanical barrier strategy for preventing IUAs recurrence post-TCRA by the European Society of Gynecologic Endoscopy (ESGE) and the American Society of Gynecologic Laparoscopists (AAGL) [7, 8]. Some subsequent randomized controlled trials revealed that HA gel did not significantly reduce IUAs recurrence rates after surgery. Additionally, no significant differences were observed in the American Fertility Society scores during the second hysteroscopy or in menstrual pattern improvements at the 3-month follow-up between the two groups [9, 10]. Thus, exploring the pathogenesis of IUAs and adopting the concept of precision medicine to achieve individualized treatment, while avoiding blind treatment, overtreatment, and ineffective treatment has important clinical and research value.

Our research group explored whether human umbilical cord mesenchymal stem cells (HUCMSCs) could serve as "shortcuts" for endometrial regeneration and repair in patients with IUAs, and we found that the CM-Dil-labelled HUCMSCs were barely distributed in the endometrial epithelium, regardless of whether they were injected via the tail vein or intraperitoneally. Instead, these cells were predominantly found in the myometrial

layer, with no statistically significant difference in distribution compared with endometrial stromal cells [11]. Some scholars have analysed the pathological characteristics of scar tissue from IUAs patients and normal myometrial tissue and found no significant difference in histological morphology between the two groups, suggesting that scar tissue may originate from the myometrium [12]. However, the interface of the myometrium-endometrium is a special zone called the uterine junction zone (JZ), which is the inner one-third of the myometrium and has a low signal intensity on MRI [13]. The physiological role of the JZ differs from that of the outer myometrium, as it is influenced by ovarian sex hormones. The JZ exhibits a cyclic pattern of oestrogen and progesterone receptor expression similar to that of the endometrium, whereas the outer myometrium does not display such a pattern [14]. The literature also shows that abnormalities in the JZ can cause a series of diseases, such as endometrial cancer, adenomyosis and infertility [15, 16]. Notably, a study revealed that the JZ is important in diagnosing IUAs, especially in predicting postoperative recovery and pregnancy outcomes [17]. On the basis of the above findings, it can be speculated that the myometrium, especially the inner myometrium possibly participates in the occurrence and progression of endometrial injury. Therefore, this study focused on the inner and outer myometrium separately.

With the emergence of high-throughput biotechnologies, the new era of "omics" big data has thoroughly propelled the study of the molecular mechanisms underlying complex phenotypes. The concept of transcriptomics, which refers to the study of gene expression and the regulation of gene transcription at the RNA level by transcribing complete gene transcripts or RNA species that are transcribed in specific cell types, tissues or organisms for specific conditions, was first proposed in 1991. The related research methods include gene chip technology, which is based on hybridization methods, and expressed sequence tag (EST) analysis and RNA sequencing (RNA-seq), which are based on high-throughput sequencing technology [18]. Proteomics, first proposed in 1994, involves comprehensive analysis of cellular proteins by mass spectrometry, two-dimensional gel electrophoresis, and bioinformatics. This approach can supplement genomic and transcriptomic methods. Proteomics is an important tool for exploring biomarkers for disease diagnosis and prognosis, new therapeutic targets, and genetic analysis [19]. The relationship between transcription products and translation products is not necessarily one-to-one, thus relying solely on transcriptomic data is insufficient to infer the expression of genes at the protein level after translation, nor can it explain the final occurrence of

biological events. Compared with single omic data analysis, multiomic analysis can compensate for missing data and confounding factors, and multiomics data can be mutually verified to reduce false positives. More importantly, multiomic joint analysis can explore biological activities at multiple levels, which is more conducive to studying the complete mechanisms of disease occurrence and therapeutic targets.

Currently, there is still a gap in the comprehensive study of the molecular regulatory mechanisms between the injured endometrium of IUAs and myometrium at both the transcriptomic and proteomic levels. Therefore, we conducted comparative analyses of the lesional tissue of IUAs (moderate and severe) and myometrium (inner and outer layers) via transcriptomics and data-independent acquisition (DIA) proteomic methods combined with bioinformatic analysis to further explore the changes in signal transduction pathways and interactions between genes and reveal potential correlations and important target pathways of differentially expressed genes and proteins in the myometrium and IUAs lesional tissue.

## Materials and methods

### Study subjects and grouping

The IUAs patients who underwent TCRA at our hospital from July 2023 to December 2023 were researched. The proliferative phase endometrium of these patients was classified into moderate (5–8 points) and severe (9–12 points) grades according to the American Fertility Society (AFS) scoring criteria. Additionally, the inner and outer myometrial tissues of patients who underwent hysterectomy for cervical intraepithelial neoplasia grade III (CIN III) or benign ovarian tumors were selected. The inclusion criteria of myometrium was: 1) Preoperative MRI revealed a normal uterine structure, a finding that was subsequently confirmed by postoperative pathological examination; 2) age between 20 and 35 years; 3) no other endocrine, breast, immune, or metabolic diseases; 4) and no hormone therapy within 3 months prior to surgery. The exclusion criteria of myometrium included diagnosed with hysterosarcoma, adenomyosis, endometriosis, endometrial cancer, and other myometrial or endometrial lesions. In summary, the research groups were divided as followed: 1) 13 IUAs lesional tissues were identified as Group B, then 5 cases of them were divided into severe (S) Group and 8 cases in moderate (M) Group; 2) 7 normal myometrium were identified as Group J and they were further divided into inner (I) Group and outer (O) Group.

### Sample collection

The handling and sectioning of tissue samples were carried out as quickly as possible on ice to prevent RNA

degradation. Tissue samples for histological analysis were fixed in formaldehyde immediately after sampling. The sampling criteria is detailed in Sects. " [Sampling of group S and M](#)" and " [Sampling of group I and O](#)".

### Sampling of group S and M

Lesional tissue from IUAs patient was collected during the proliferative phase (3–7 days after the menstrual period), without sexual intercourse and vaginitis. The sample was about 0.5 cm × 0.5 cm × 0.1 cm in size and being placed into pre-chilled RNase-free sterile cryovials with screw caps, immediately frozen in liquid nitrogen for at least 15 min, then transferred to –80 °C freezer waiting for testing.

### Sampling of group I and O

Given the absence of endometrial tissue beneath the JZ, the basal layer of the endometrium is directly adjacent to the myometrium, and there are no distinct histological characteristics to distinguish the JZ from the outer myometrium under the microscope to date. In line with the research methods of Mehassed et al. [16], sampling was performed by fixing the middle part of the anterior uterine wall. Firstly, the endometrium was gently scraped off. Then, the tissue 5–8 mm below the basal layer of the endometrium was identified as inner myometrium, and the inner half of the inner myometrium was collected as Group I. Similarly, the outer one-third of the myometrium was identified as outer myometrium, and the outer half of the outer myometrium was selected as Group O, avoiding the influence of the transitional zone on the selection of the field of view. The preservation of sample was similar to Sect. " [Sampling of group S and M](#)".

### Histological staining

Hematoxylin and eosin (H&E) staining was used to observe tissue morphology. Masson's trichrome staining was used to assess the fibrosis within groups.  $\alpha$ -Smooth muscle actin ( $\alpha$ -SMA) and H-caldesmon as markers for smooth muscle cells, were subjected to immunohistochemistry (IHC) staining to preliminarily explore the relationship between IUAs and myometrium. For the results of Masson's staining, five independent sections with a magnification of ×100 were randomly selected, and the fibrotic area was calculated using ImageJ software. For the IHC staining results of  $\alpha$ -SMA and H-caldesmon, five independent sections with a magnification of ×100 were randomly selected, and the average optical density (AOD) was calculated with ImageJ software.

## Transcriptomics analysis

### RNA sequencing

Firstly, using TRIzol Reagent extracted total RNA from samples. The concentration and purity of the extracted RNA were assessed with the Agilent 2100 Bioanalyzer and RNA-specific agarose gel electrophoresis. Next, PolyA-structured mRNA was enriched from the total RNA using oligo (dT) magnetic beads, RNA was fragmented by ionization to fragments of approximately 300 base pairs (bp) in length, then cDNA was synthesized using RNA as a template. After the construction of the library, PCR amplification was used to enrich the library fragments, followed by selecting fragments with 450 bp. Then the quality and the total concentration and effective concentration of the library were measured by the Agilent 2100 Bioanalyzer. After RNA extraction, purification, and library construction, the second-generation sequencing technology (NGS) was used to perform paired-end (PE) sequencing of these libraries, based on the Illumina sequencing platform.

### Analysis of differentially expressed genes

First, check the correlation of gene expression levels between samples, represented by the Pearson correlation coefficient. Generally, a correlation coefficient between 0.6 and 1 is considered strong. Principal component analysis (PCA) was performed on the samples based on expression levels, and differential gene expression analysis was conducted using the R language DESeq package. The R language ggplot2 package was used to draw a volcano plot of differentially expressed genes (DEGs) to display the gene distribution, the fold change in gene expression, and the significance of the results. Based on the results of the differential analysis, the number of differential genes between each comparison group was counted. The R language Pheatmap package was used for two-way hierarchical clustering analysis of the union of DEGs from all comparison groups, clustering based on the expression levels of the same gene in different samples and the expression patterns of different genes in the same sample, using the Euclidean method to calculate distances, and hierarchical clustering with the longest distance (Complete Linkage) for clustering.

## Proteomics analysis

### DIA proteomics analysis

Peptide sequences of tissues from each group were identified using liquid chromatography-tandem mass spectrometry (LC-MS/MS) to proteomics analysis. Some protein sample from each case was used to construct a Spectral Library. The consistency between samples was assessed by SDS-PAGE electrophoresis for each group. All samples were digested with Trypsin using the FASP

method. Peptide concentration was determined by OD280 measurement, and fractions were collected using the HPRP method. 2 µg peptides mixed with appropriate iRT standard peptides were detected by DDA mass spectrometry. Chromatographic separation was performed using a nanoflow HPLC system nanoElute (Bruker Daltonics). Samples separated by liquid chromatography were subjected to timsTOF Pro (Bruker) mass spectrometry. Maxquant software was used to process the acquired mass spectrometry data, with the database being the Mus musculus\_uniprot downloaded database. Parameters were set as followed: enzyme was trypsin, max missed cleavage site was 2, fixed modification was Carbamidomethyl (C), and dynamic modifications were set to Oxidation (M) and Acetyl (Protein N-term), with protein identification from the database search using the filter parameters FDR < 1%. The original raw files and search results were imported into the Maxquant software to build a Spectral Library. Each sample underwent DIA mass spectrometry detection, with chromatographic separation performed using a nanoflow HPLC system nanoElute, with the same liquid chromatography gradient and DDA test as before. Samples separated by nanoscale high-performance liquid chromatography were subjected to DIA mass spectrometry analysis using the timsTOF Pro mass spectrometer, with MS2 adopting the DIA data acquisition mode. Maxquant software was used for data processing, with the database being the same as that used for library construction.

### Analysis of differentially expressed proteins

Firstly, using R language ggplots2 package drew a volcano plot of differentially expressed proteins (DEPs) to display the protein distribution, the fold change in protein expression, and the significance of the results. Based on the results of the differential analysis, the number of DEPs within each comparison group was counted. The R language pheatmap package was used for two-way hierarchical clustering analysis of the union of DEPs from all comparison groups, clustering based on the expression levels of the same protein in different samples and the expression patterns of different proteins in the same sample, using the Euclidean method to calculate distances, and hierarchical clustering with the longest distance (Complete Linkage) for clustering.

## Correlation analysis of transcriptomics and proteomics

Integrate the overall data from transcriptomics and proteomics for a correlation analysis to identify DEGs and DEPs and either upregulated or downregulated in both sequencings. By combining the sets of genes and proteins that upregulated or downregulated, the intersection of co-expressed genes and proteins can be determined and

presented using a Venn diagram. A correlation coefficient analysis was conducted to assess the relationship between the DEGs and DEPs. The DEGs and DEPs were then analyzed for Gene Ontology (GO) functional enrichment and Kyoto Encyclopedia of Genes and Genomes (KEGG) pathway enrichment. Utilizing the STRING database, the direct and indirect interactions between the DEGs and DEPs were explored to construct Protein-Protein Interaction Networks (PPI), with a focus on identifying proteins that had a higher degree of connectivity.

**Statistical analysis**

GraphPad Prism 8.0 statistical analysis software was used to perform the statistical processing of the data. Continuous variables that conform to the normal distribution were expressed as the mean ± standard deviation ( $\bar{X} \pm S$ ), while non-normally distributed data were represented using the median (M(P25, P75)). In the analysis of significant differences in gene and protein expression, the default method was combining the Student's t-test with the fold change (FC, the ratio of the average expression of two groups) to identify significantly DEGs and DEPs ( $p < 0.05$ , and  $FC > 2$  or  $< 0.5$ ). The GO and KEGG database analyses were based on the algorithm of Fisher's exact test for functional and pathway enrichment analysis of the annotation results,  $p < 0.05$  was considered significant enrichment, with a smaller value indicating more significant enrichment.

**Results**

**Basic clinical characteristics of patients**

In this study, a total of 20 patients were included. The patients in Group J, Group I and Group O were same. The average age of Group B was  $33.46 \pm 3.62$  years, Group J was 37 (33.5, 37) years. The average number of gravidity in Group B was  $3.23 \pm 1.69$ , Group J was  $3.43 \pm 1.27$ . The average number of abortion in Group B was 2.00 (1.00, 2.00), Group J was  $1.14 \pm 1.21$ . The comparison between Group B and Group J showed no significant difference in age, gravidity and abortion ( $P > 0.05$ ) (Table 1). Group B was further divided into Group S (5 cases) and Group M (8 cases). Group S had an average age of  $33.80 \pm 1.92$  years, average number of gravidity  $3.00 \pm 1.00$

**Table 1** Comparison of baseline clinical data between B and J group

	<b>B Group (n=13)</b> $\bar{X} \pm S / M(P25, P75)$	<b>J Group (n=7)</b> $\bar{X} \pm S / M(P25, P75)$	<b>t/Z</b>	<b>P</b>
Age (years)	$33.46 \pm 3.62$	37(33.5, 37)	-1.517	0.129
Gravidity	$3.23 \pm 1.69$	$3.43 \pm 1.27$	-0.270	0.790
Abortion	2.00(1.00, 2.00)	$1.14 \pm 1.21$	-1.440	0.150

and abortion 2.00 (1.00, 2.00). The comparison between Group S and Group J showed no significant difference in age, gravidity and abortion ( $P > 0.05$ ) (Table 2). Group M had an average age of  $33.25 \pm 4.50$  years, average number of gravidity  $3.38 \pm 2.07$  and abortion  $2.38 \pm 1.51$ . The comparison between Group M and Group J also showed no significant difference in age, gravidity and abortion ( $P > 0.05$ ) (Table 3).

**Histologic features**

H&E staining was used to observe the morphological characteristics of tissues in each group. The uterine muscle cells in Group I and O were neatly arranged with dense intercellular structures (Fig. 1A). Group M and S showed sparsely arranged smooth muscle fibers, Group S displayed morphological characteristics of smooth muscle tissue, while Group M showed little residual endometrial tissue. Masson's trichrome staining was used to observe the degree of fibrosis in each group. The blue staining corresponds to collagen fibers, and the areas of fibrosis in Group M and S were similar to that of Group I and significantly increased compared to Group O (Fig. 1A). Statistical analysis revealed that there was no statistically significant difference in fibrosis area between Group M and S compared to Group I ( $P > 0.05$ ), but the fibrosis area in Group M and S was significantly higher than that in Group O, with a statistically significant difference ( $P < 0.05$ ) (Fig. 1B).  $\alpha$ -SMA and H-caldesmon are markers of smooth muscle tissue, brown cytoplasm indicates positive staining (Fig. 1A). Statistical analysis showed that the expression of  $\alpha$ -SMA in Group M were significantly lower than in Group I and Group O, with a

**Table 2** Comparison of baseline clinical data between S and J Group

	<b>S Group (n=5)</b> $\bar{X} \pm S / M(P25, P75)$	<b>J Group (n=7)</b> $\bar{X} \pm S / M(P25, P75)$	<b>t/Z</b>	<b>P</b>
Age (years)	$33.80 \pm 1.92$	37(33.5, 37)	-1.320	0.187
Gravidity	$3.00 \pm 1.00$	$3.43 \pm 1.27$	-0.625	0.546
Abortion	2.00(1.00, 2.00)	$1.14 \pm 1.21$	-0.769	0.442

**Table 3** Comparison of baseline clinical data between M and J group

	<b>M Group (n=8)</b> $\bar{X} \pm S / M(P25, P75)$	<b>J Group (n=7)</b> $\bar{X} \pm S / M(P25, P75)$	<b>t/Z</b>	<b>P</b>
Age (years)	$33.25 \pm 4.50$	37(33.5, 37)	-1.283	0.199
Gravidity	$3.38 \pm 2.07$	$3.43 \pm 1.27$	-0.059	0.954
Abortion	$2.38 \pm 1.51$	$1.14 \pm 1.21$	1.726	0.108

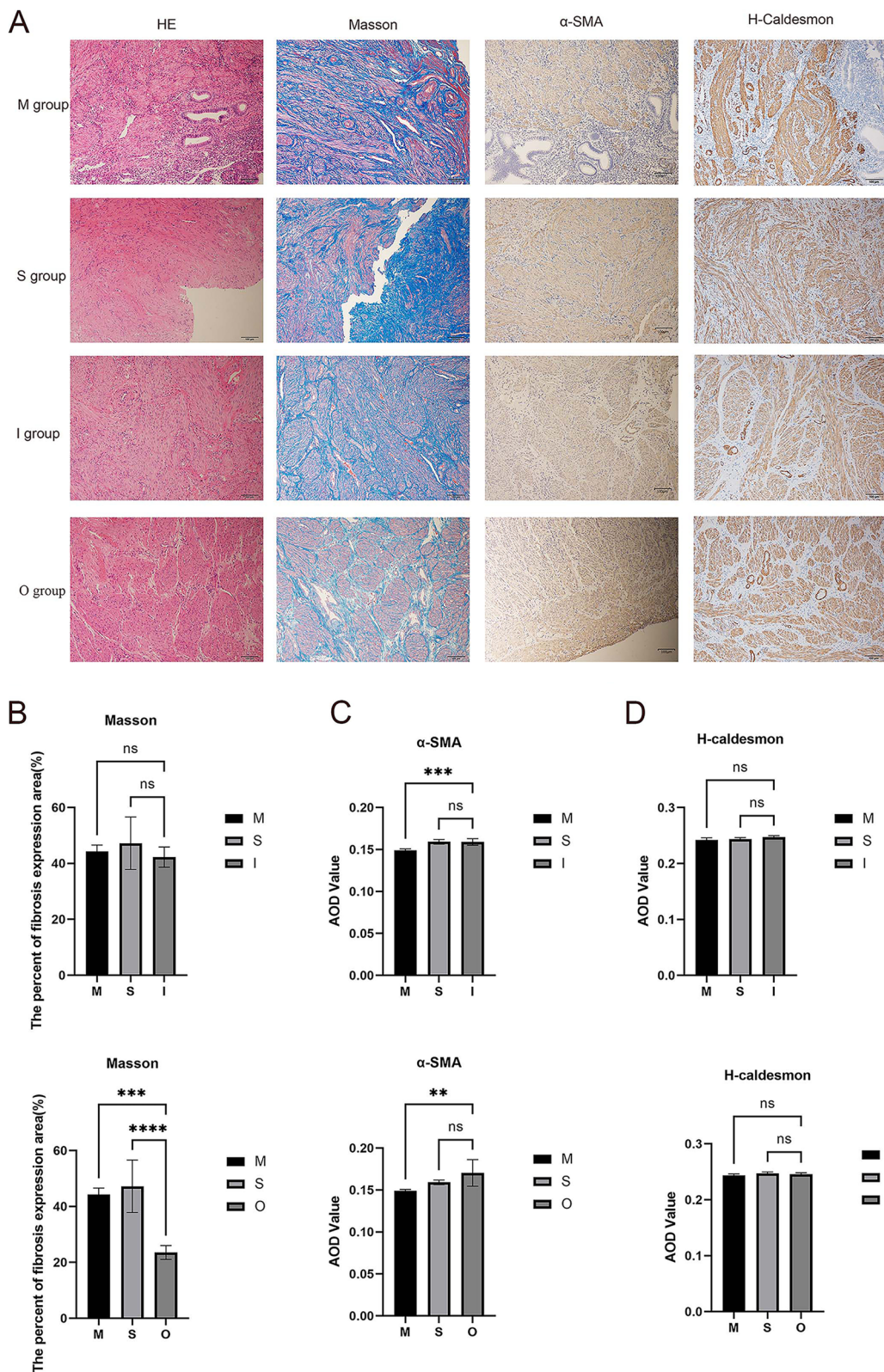


**Fig. 1** Morphological characteristics. **A** HE staining, Masson's trichrome staining and immunohistochemical staining of α-SMA, and H-caldesmon in each group. Scale bar 100 μm. **B** Quantification of the fibrosis area percentage. **C-D** Quantification of expression of α-SMA and H-caldesmon. Data were shown as mean ± SD,  $n=5$ , ns  $P>0.05$ ,  $**P<0.01$ ,  $***P<0.001$ ,  $****P<0.0001$

statistically significant difference ( $P < 0.05$ ), while there was no statistically significant difference between Group S and both Group I and O ( $P > 0.05$ ) (Fig. 1C). And the expression of H-caldesmon in both Groups M and S was not statistically significantly different with Group I and O ( $P > 0.05$ ) (Fig. 1D).

**Transcriptome results**

**DEGs in IUAs tissues**

To understand the pathogenesis of IUAs and its relationship with myometrium, we conducted transcriptome analysis on Groups B, S, M, J, I, and O. The correlation of gene expression levels between samples is an important indicator to test the reliability of the experiment and the rationality of sample selection. The sample correlation test results showed that the correlation coefficients within each sample of Group B vs. J (Fig. 2A), Group B vs. I vs. O (Fig. 2B) and Group S vs. M vs. I vs. O (Fig. 2C) were all beyond 0.65, indicating a strong correlation, which suggests good reliability of the test. Additionally, PCA analysis can cluster similar samples together, with closer distances indicating higher similarity among samples: Group B vs. J (Fig. 2D), Group B vs. I vs. O (Fig. 2E) and Group S vs. M vs. I vs. O (Fig. 2F).

DEGs were screened to investigate the potential functions and targeted pathways related to myometrium and IUAs lesional tissue. Among all annotated genes, compared to Group J, Group B's transcriptome analysis identified a total of 3,619 DEGs, with 1,315 up-regulated genes and 2,304 down-regulated genes (Fig. 3A,

3B). Compared to Group I, Group B identified a total of 2,948 DEGs, with 931 up-regulated genes and 2,017 down-regulated genes (Fig. 3A, 3C). Compared to Group O, Group B identified a total of 4,010 DEGs, with 1,581 up-regulated genes and 2,429 down-regulated genes (Fig. 3A, 3D). Compared to Group I, Group S identified a total of 2,771 DEGs, with 1,713 up-regulated genes and 1,058 down-regulated genes (Fig. 3A, 3E). Compared to Group I, Group M identified a total of 2,791 DEGs, with 1,894 up-regulated genes and 897 down-regulated genes (Fig. 3A, 3F).

**Proteomics results**

**DEPs in IUAs tissues**

DEPs were also screened to investigate the potential functions and targeted pathways related to myometrium and IUAs lesional tissue. Among all annotated proteins, compared to Group J, Group B's proteomic analysis identified a total of 901 DEPs, with 126 up-regulated and 593 down-regulated (Fig. 4A, 4B). Compared to Group I, Group B identified 795 DEPs, with 93 up-regulated and 472 down-regulated (Fig. 4A, 4C). Compared to Group O, Group B identified 1216 DEPs, with 230 up-regulated and 682 down-regulated (Fig. 4A, 4D). Compared to Group I, Group S identified 902 DEPs, with 62 up-regulated and 398 down-regulated (Fig. 4A, 4E). Compared to Group I, Group M identified 942 DEPs, with 173 up-regulated and 513 down-regulated (Fig. 4A, 4F).

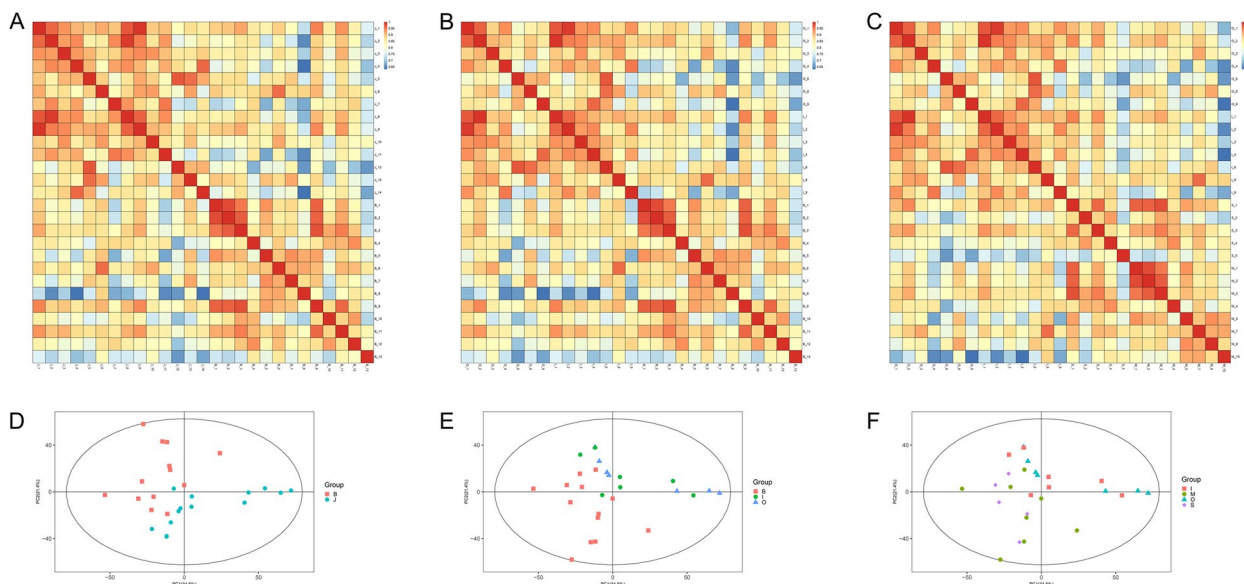


**Fig. 2** Analysis of gene expression in each group. **A-C** Sample correlation test. Group B vs. J (**A**), Group B vs. I vs. O (**B**) and Group S vs. M vs. I vs. O (**C**). The squares of different colors represent the high or low correlation between the groups. **D-F** PCA analysis. Group B vs. J (**D**), Group B vs. I vs. O (**E**) and Group S vs. M vs. I vs. O (**F**). Different shapes in the figure indicate different samples, and different colors indicate different groups

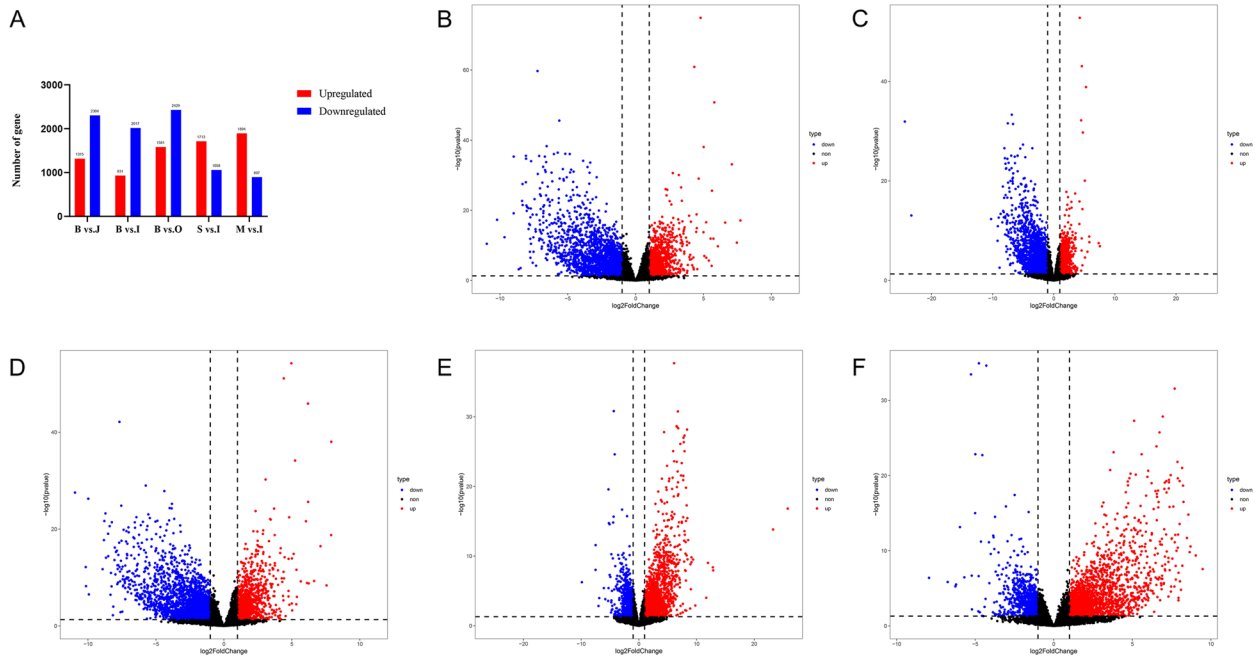


**Fig. 3** Analysis of DEGs. **A** Bar graph of the results of differential expression analysis. **B-F** Volcano plot of DEGs in the comparison groups of BvsJ (**B**), BvsI (**C**), BvsO (**D**), Svsl (**E**), and Mvsl (**F**). The abscissa is log2FoldChange, and the ordinate is  $-\log_{10}$  (p-value). Up-regulated genes are shown in red and down-regulated genes in blue

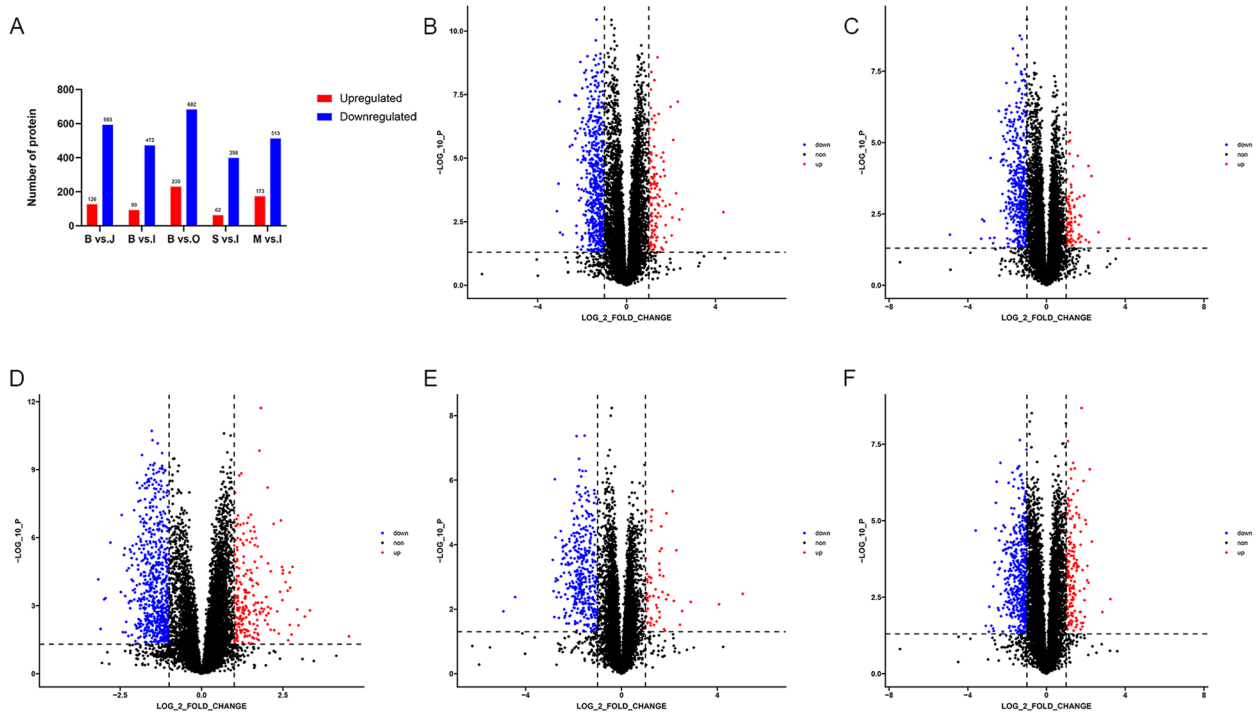


**Fig. 4** Analysis of DEPs. **A** Bar graph of the results of differential expression analysis. **B-F** Volcano plot of DEPs in the five comparison groups of BvsJ (**B**), BvsI (**C**), BvsO (**D**), Svsl (**E**), and Mvsl (**F**). The abscissa is log2FoldChange, and the ordinate is  $-\log_{10}$  (p-value). Up-regulated genes are shown in red and down-regulated genes in blue

### Integrated analysis of transcriptomic and proteomic results

The integrated transcriptomic and proteomic analysis as depicted in the Venn diagrams (Fig. 5A, 5B). The correlation analysis reveals distinct patterns of mRNA and protein regulation across various groups. Group J and B exhibited 4 up-regulated and 22 down-regulated mRNA or protein enriched into the same pathway. The number in Group I and B were respectively 3 up-regulated and 20 down-regulated, in Group O and B were respectively 4 up-regulated and 24 down-regulated, in Group I and S were respectively 13 up-regulated and 14 down-regulated, and in Group I and M were respectively 41 up-regulated and 59 down-regulated (Fig. 5A, 5B). The heatmap of the correlation analysis revealed that the DEGs and DEPs identified exhibit a significant correlation, which were statistically significant (Fig. 5C).

### GO enrichment analysis of DEGs and DEPs

The GO enrichment analysis showed the molecular function, biological processes and cellular components of DEGs and DEPs enriched into the same pathway in each comparison group (Fig. 5D). Compared to Group J, the DEGs and DEPs in Group B mainly enriched in regulating immune response, cell proliferation and differentiation, as well as integrin activation. For example, the molecular functions (MF) of DEGs and DEPs in Group B mainly enriched in microtubule motor activity, type I transforming growth factor beta (TGF- $\beta$ 1) receptor binding, type II transforming growth factor beta receptor (TGF- $\beta$ 2) binding, plus-end-directed microtubule motor activity, protein transmembrane transporter activity, peptide antigen binding, microtubule binding, scaffold protein binding, hyaluronic acid binding, and tubulin binding. They were involved in biological processes (BP) such as positive regulation of interleukin-1 production, immunoglobulin production, immune response, epithelial cell proliferation involved in wound healing and stem cell differentiation. They also regulated integrin activation, complement activation, immune system process, wound healing, stem cell division, spreading of epidermal cells and stem cell proliferation. These DEGs and DEPs were mainly located in cellular components (CC) such as extracellular exosome, extracellular region, collagen-containing extracellular matrix (ECM), platelet alpha granule lumen, microtubule associated complex, spindle microtubule, and kinesin complex.

When control Group J was further divided into Group I and O, we found that the DEGs and DEPs in Group B also primarily enriched in immune response, cell proliferation and differentiation, as well as integrin activation. As followed, compared to Group I, the MF of DEGs and DEPs in Group B were most similar to compared to Group J. It mainly enriched in TGF- $\beta$ 1 receptor binding,

TGF- $\beta$ 2 receptor binding, plus-end-directed microtubule motor activity, MHC class I protein binding, and tubulin binding. The BP involved except for that in compared with Group J, also included positive regulation of TGF- $\beta$  receptor signalling pathway and morphogenesis of an epithelium. The location in CC of these DEGs and DEPs was same as comparison Group B and J. Compared to Group O, while the MF involved was different, it mainly enriched in hyaluronic acid binding, mechanosensitive ion channel activity, protein transmembrane transporter activity, phosphoprotein binding, and scaffold protein binding. BP added hyaluronan metabolic process. CC involved was same.

Then, Group I served as the control group, Group B was further divided into Group S and Group M to detect the potential relationship between the severity of IUAs and myometrium. The results showed that the DEGs and DEPs in Group S primarily enriched in regulation of cell proliferation, differentiation, and migration, the coagulation cascade system, immune response, and reorganization of the actin filament cytoskeleton. For instance, the MF in Group S mainly enriched in actin filament binding, calcium ion binding, heparin binding, microtubule binding, myosin light chain binding, heparan sulfate proteoglycan binding, protein-containing complex binding, TGF- $\beta$  binding, microfilament motor activity, structural constituent of muscle, and hyaluronic acid binding. The BP involved included blood coagulation, complement activation, actin filament organization, myoblast migration, muscle filament sliding, tissue remodelling, and production of molecular mediators involved in the inflammatory response, as well as positive regulation of T cell proliferation, endothelial cell proliferation, cell migration, and actin filament depolymerization. The location in CC contained extracellular exosome, extracellular region, cortical actin cytoskeleton, platelet alpha granule lumen, collagen-containing ECM, protein-containing complex, ECM, platelet dense granule lumen, muscle myosin complex, platelet alpha granule membrane, myosin II complex, myosin filament, microtubule-associated complex, spindle microtubule, sarcoplasmic reticulum, sarcomere, cell periphery, and microtubule. Additionally, in Group M, the enrichment pathway was related to the regulation of cell proliferation and migration, immune response, and reorganization of the actin filament cytoskeleton. The MF enriched in myosin heavy chain binding, MHC-II receptor activity, efflux transmembrane transporter activity, myosin light chain binding, Wnt-protein binding, Wnt receptor activity, filamin binding, structural constituent of muscle, ECM structural constituent conferring compression resistance, microfilament motor activity, and GTP-dependent protein binding. The BP of them was involved in positive regulation

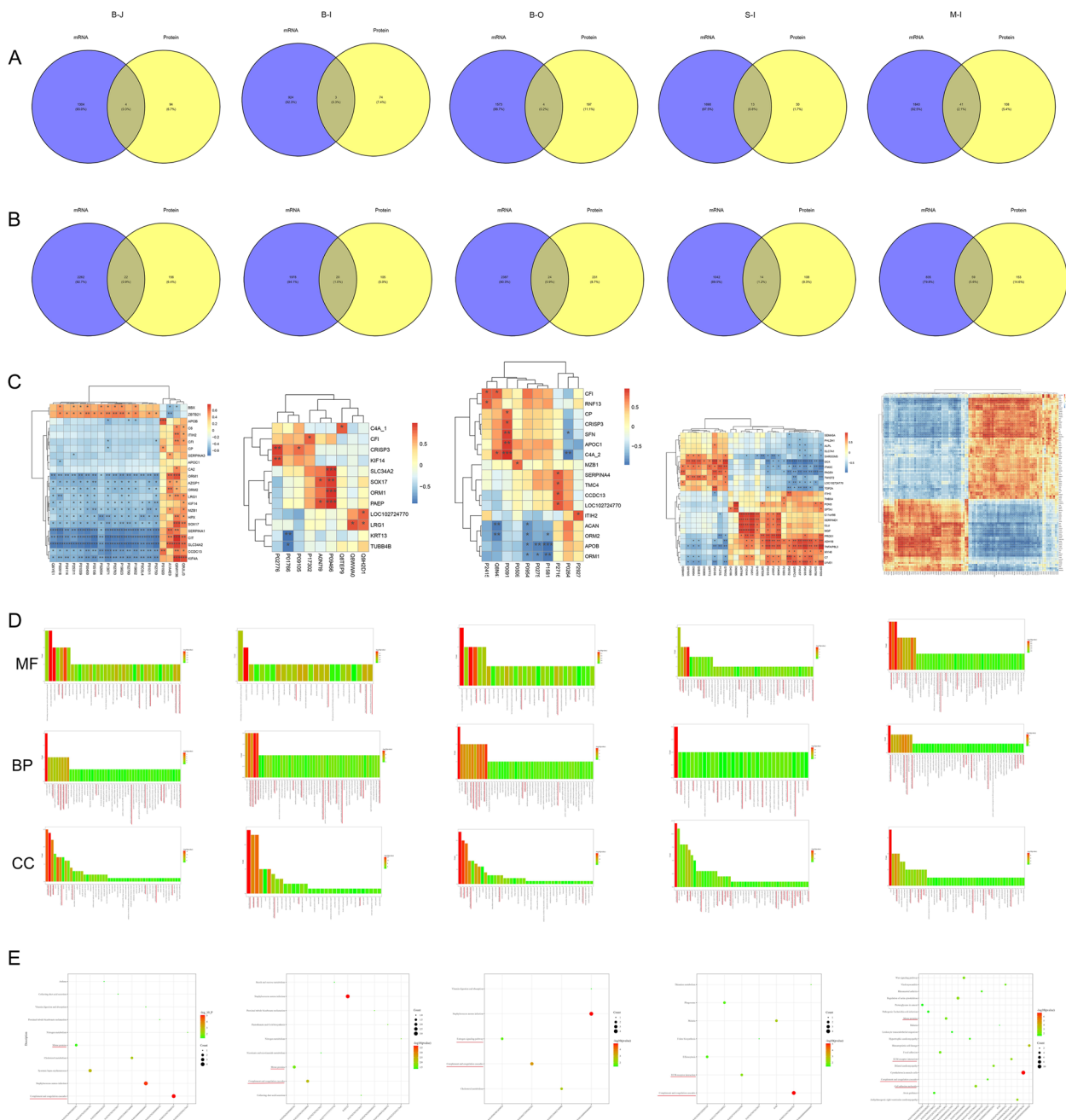


**Fig. 5** Combined analysis of transcriptome and metabolome data. **A** Number of up-regulated DEGs and DEPs enriched into the same pathway. **B** Number of down-regulated DEGs and DEPs enriched into the same pathway. **C** Heatmap of correlation between DEGs and DEPs in each comparison group. **D** GO function enrichment analyses of DEGs and DEPs enriched into the same pathway in each comparison group. **E** KEGG pathway enrichment analysis of coexpression DEGs and DEPs in each comparison group. **D** and **E** showed the data with  $P < 0.05$  and the top 50 values of the rich-factor

of epithelial cell proliferation involved in wound healing, actin filament depolymerization and CD4+ T cell-mediated immunity, negative regulation of calcium ion transport, as well as regulation of somatic stem cell division, myoblast migration, Wnt signalling pathway, planar cell

polarity pathway, ryanodine-sensitive calcium-release channel activity, muscle filament sliding, T cell migration, and tissue remodelling. These DEGs and DEPs were primarily located in CC such as muscle myosin complex, junctional sarcoplasmic reticulum membrane,

sarcoplasmic reticulum, myosin II complex, platelet alpha granule membrane, cell–cell contact zone, myosin filament, cortical actin cytoskeleton, myofibril, stress fiber, and microtubule-associated complex.

#### **KEGG enrichment analysis of DEGs and DEPs**

The KEGG analysis showed the same enrichment pathway of the DEGs and DEPs in each comparison group (Fig. 5E). Compared to Group J, the DEGs and DEPs in Group B mainly enriched in the pathway of Complement and coagulation cascades, and Motor proteins. The detailed DEGs or DEPs in Complement and coagulation cascades were as followed, Complement component C4A, C6, and Complement factor I (CFI) covalent binding to immunoglobulins and immune complexes, playing a key role in regulating innate and adaptive immune responses. Alpha-1-antitrypsin irreversibly inhibited trypsin, chymotrypsin, and plasminogen activator to shorten the coagulation time. In addition, the Motor proteins were Kinesin-like protein KIF14, Chromosome-associated kinesin KIF4A, mainly involved in regulating cell cycle progression and cell division to regulate cell growth.

Similarly, the control Group J was further divided into Group I and Group O in KEGG analysis. Compared to Group I, the DEGs and DEPs in Group B also enriched in the pathway of Complement and coagulation cascades, and Motor proteins. Apart from above genes or proteins, Tubulin beta-4B chain was also included, which primarily involved in the composition of microtubules. While compared to Group O, the enrichment pathway were Complement and coagulation cascades and Estrogen signalling pathway. Among the DEGs and DEPs, Keratin, type I cytoskeletal 17, which involved in promoting the proliferation of epithelial cells deserved attention.

Next, Group I served as the control group, Group B was further divided into Group S and Group M. Compared to Group I, the DEGs and DEPs in Group S mainly enriched in the pathway of Complement and coagulation cascades, and ECM-receptor interaction. The detailed DEGs or DEPs mainly included Complement component C7, which involved in complement activation. Vitamin K-dependent protein S and Heparin cofactor 2 (HCII), which primarily involved in preventing coagulation and stimulating fibrinolysis. Platelet glycoprotein 4 and Thrombospondin-4 (TSP-4) were involved in intercellular and cell–matrix interactions, including cell proliferation, migration, adhesion, and attachment. In Group M, the enrichment pathway was the most, besides of Complement and coagulation cascades, and ECM-receptor interaction, there were also the Motor proteins, Cell adhesion molecule, and Leukocyte transendothelial migration. So apart from Complement component C7

and TSP-4, the DEGs and DEPs also contained Integrin alpha-IIb, which triggered platelet/platelet interactions by binding to soluble fibrinogen, leading to rapid platelet aggregation. Basement membrane-specific heparan sulfate proteoglycan core protein, which served as an attachment matrix for cells and is involved in angiogenesis. The Motor proteins contained Dynein axonemal heavy chain 6 exerting force towards the minus end of microtubules., as well as Tubulin beta-3 chain (a major component of microtubules), Myosin-8, and Myosin regulatory light polypeptide 9 involved in muscle contraction. Moreover, Neuronal growth regulator 1 involved in cell adhesion. HLA class II histocompatibility antigen, DQ alpha 1 chain, and Integrin alpha-L involved in various immune response. Unconventional myosin-Ig detects rare antigen-presenting cells by regulating T cell migration. Integrin alpha-X (ITGAX) mediates intercellular interactions during inflammatory responses and regulates the adhesion and chemotaxis of monocytes.

#### **PPI network analysis**

The DEPs identified through correlation analysis were visualized on a PPI network to analyze their interactions and identify key proteins co-expressed in both transcriptomic and proteomic analysis. The key proteins for the five comparison groups were 16, 11, 15, 14, and 100 respectively. For the B-J groups, 16 proteins corresponding to genes such as APOB, APOC1, AZGP1, C6, CFI, CIT, CP, HPX, ITIH2, KIF14, KIF4A, LRG1, ORM1, SERPINA1, SERPINA3, and ORM2 were found to be in central positions of the network (Fig. 6A). They primarily involved in complement activation, cell division and proliferation, regulation of hyaluronic acid synthesis and degradation, immune system activity, coagulation cascade, and transport of blood proteins. For the B-I groups, C4A, CA2, CFI, CP, HPX, LRG1, ORM1, ORM2, PAEP, PIGR, and SLPI were in central positions of the network (Fig. 6B). They mainly involved in the activation of the classical complement pathway, regulation of immune system, and transport of blood proteins. In the B-O groups, ACAN, APOB, APOC1, AZGP1, C4A, CFI, CFP, CP, HPX, ITIH2, ORM1, ORM2, SERPINA1, SERPINA4, and SHBG were central in the network (Fig. 6C). Their functions were similar to B-J groups, added to regulation of plasma metabolism of steroid hormones. For the S-I groups, ALPL, CAPN6, CD36, DCX, ADH1B, C7, CLU, ITIH3, LYVE1, MGP, PON3, PROS1, THBS4, and TNFAIP8L3 were central in the network (Fig. 6D). They mainly involved in regulating microtubule dynamics and microtubule stabilization in cell skeleton organization, cell–cell and cell–matrix interactions, immune responses through the classical complement pathway, regulation of hyaluronic acid

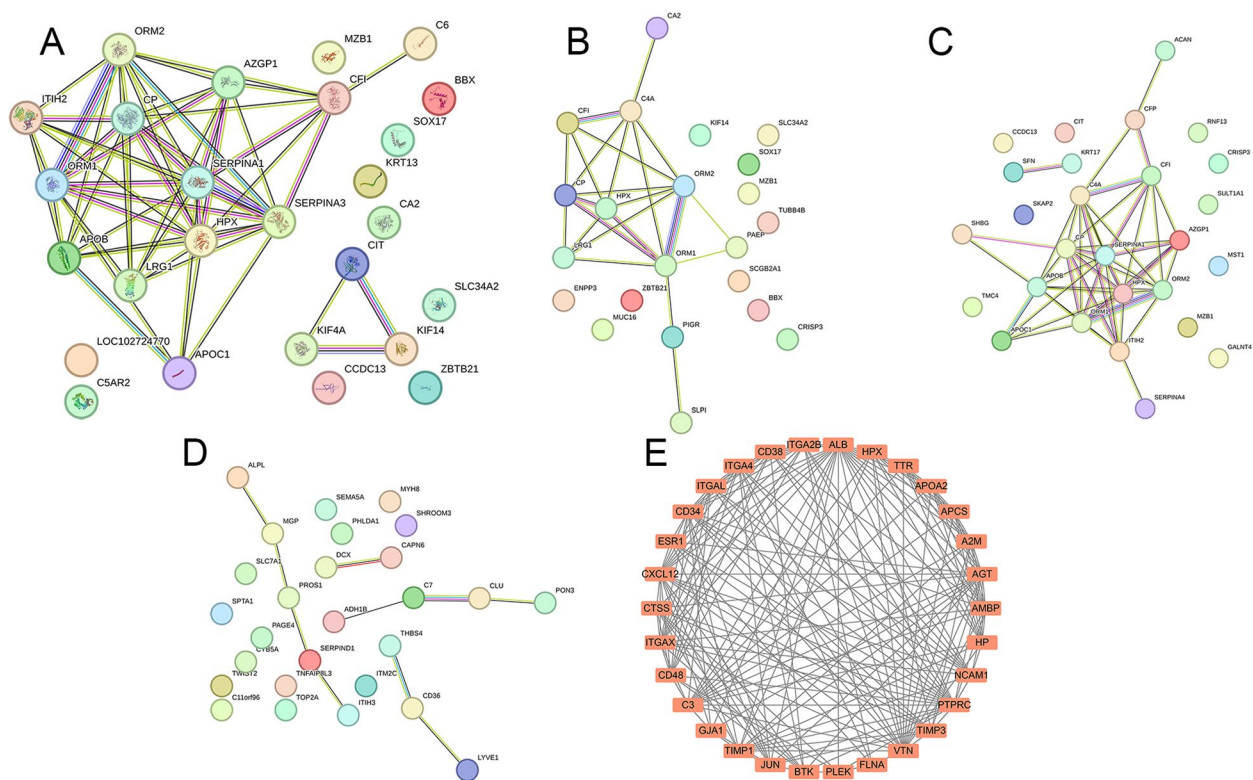


**Fig. 6** Mapping of protein partners for five comparison groups, (A-D) The protein interaction map showed direct as well as predicted protein partners of DEPs in comparison groups of BvsJ, BvsI, BvsO and Svsl. E The protein interaction map showed direct as well as predicted protein partners of top 30 DEPs in comparison group of MvsI

positioning, synthesis and degradation, lipid metabolism regulation, prevention of coagulation and stimulation of fibrinolysis, mediating cell–cell and cell–matrix interactions. For the M-I groups, ALB, PTPRC, VTN, AGT, JUN, CD34, AMBP, C3, ESR1, HP, CXCL12, A2M, FLNA, ITGA2B, NCAM1, TIMP1, ITGA4, APCS, TTR, ITGAL, GJA1, CTSS, APOA2, HPX, ITGAX, TIMP3, CD48, PLEK, CD38, and BTK were the top 30 genes central in the network (Fig. 6E). They primarily involved in the classical and alternative complement pathways, regulating cell proliferation, differentiation, migration, adhesion and death, participating in steroid hormones and their receptors cell, promoting platelet aggregation, regulation of T-cell activation, and involvement in various immune phenomena, like leukocyte-endothelial cell interactions, cytotoxic T-cell-mediated killing, antibody-dependent killing of granulocytes and monocytes, leukocyte adhesion and transport. Integrating the results of transcriptomics and proteomics, and by searching for the functions of the corresponding genes or proteins in UniProt, we have identified the key genes or proteins and the pathways in each group comparison (Table 4).

### Discussion

In patients with moderate to severe IUAs, the repair of the functional endometrium poses a major challenge. Elucidating the pathogenesis of IUAs is crucial for advancing targeted treatments. Some studies have shown that endometrial fibrosis is caused by endothelial cells promoting the appearance of fibroblasts during IUAs through the endometrial-to-mesenchymal transition [20]. Another research team reported that decreased CXCL5 expression in IUAs patients leads to the downregulation of MMP9, which plays a key role in the degradation of the ECM and fibrous tissue, and its low expression may lead to excessive deposition of the ECM, thereby promoting endometrial fibrosis and adhesion formation [21]. Additionally, a study revealed that IL-33 is involved in the pathogenesis of IUAs by stimulating the phosphorylation of c-Jun N-terminal kinase (JNK), extracellular signal-regulated kinase (ERK) and p38, which are components of the MAPK signalling pathway. Anti-IL-33 treatment can inhibit the activation/phosphorylation of JNK, ERK and p38, reduce the production of inflammatory factors, and promote the fertility of IUAs model mice, which

**Table 4** Identified key genes or proteins, and the enrichment pathways in each comparison groups

	Genes or Proteins	Pathway
B-J group	KIF14, KIF4A, CIT, C4-A, C6, CFI, ORM1, ORM2, Alpha-1-antitrypsin, CP, HPX	Complement and coagulation cascades, Motor proteins
B-I group	KIF14, Tubulin beta-4B chain, C4-A, CFI, ORM1, ORM2, PAEP, PIGR, SLPI, CP, HPX	Complement and coagulation cascades, Motor proteins
B-O group	C4-A, CFI, CFP, ORM1, ORM2, CP, HPX, SERPINA1, ITIH2	Complement and coagulation cascades, Estrogen signaling pathway
S-I group	C7, PROS1, Heparin cofactor 2, CLU, CD36, THBS4, ITIH2	Complement and coagulation cascades, Estrogen signaling pathway
M-I group	HLA-DQA1, Unconventional myosin-Ig, ITGAL, ITGAX, PTPRC, CD48, CD38, BTK, CXCL12, C7, C3, HP, HPX, AMBP, PLEK, ITGA2B, ITGA4, and CD34, THBS4, Neuronal growth regulator 1, VTN, TIMP1, TIMP3, ESR1, Basement membrane-specific heparan sulfate proteoglycan core protein	ECM-receptor interaction, Cell adhesion molecules, Motor proteins, Complement and coagulation cascades, Leukocyte transendothelial migration

provides a new strategy for the prevention and clinical treatment of IUAs [22]. The pathogenesis of IUAs is complex and diverse. In this study, through combined transcriptomic and proteomic analysis, we determined that the inhibition of mitosis in endometrial cells may be an important mechanism leading to the occurrence of IUAs. In addition, imbalances in the immune coagulation cascade and extracellular matrix remodelling are related to the development of IUAs.

In this study, compared with Group I, Group B presented fewer DEGs and DEPs than compared with Group J. These findings support the notion that IUAs lesional tissue is more closely related to the inner myometrium than to the total myometrium. Immunohistochemical analysis revealed that both the IUAs lesional tissue and the uterine myometrium expressed smooth muscle cell markers. The histopathological staining results indicated that Groups M and S have fibrotic manifestations and histological characteristics of smooth muscle cells similar to those of Group I. There was no significant difference in the expression of  $\alpha$ -SMA between Groups S and I. This finding was consistent with the findings of Li W. et al., who also reported no significant differences in tissue morphology or  $\alpha$ -SMA expression between the scar tissue of the IUAs and the normal uterine myometrium [9]. Therefore, the scar tissue of the IUAs may primarily originate from the myometrium rather than the endometrium. This finding also explains our previous results that the CM-Dil-labelled HUCMSCs were predominantly distributed in the myometrial layer rather than the endometrial epithelium after injection into rats for treatment of IUA. Therefore, we need to focus on scar tissue in the uterine myometrium in addition to promoting endometrial regeneration for IUAs.

CIT, KIF14, KIF4A, and TUBB3 were downregulated in Group B compared with Group J. Previous research has indicated that all four genes are involved in the process of cytokinesis. Cytokinesis is the physical division phase

of cell division, and involves the replication and spatial separation of genetic material. In animal cells, cytokinesis involves the formation of a complex microtubule structure known as the central spindle, which forms as chromosomes regress to interphase and recruits many proteins that are crucial for the process of mitosis [23]. The downstream protein of CIT is CITK, a serine/threonine kinase of the AGC family, that plays a catalytic role in cytokinesis. CITK is localized and promotes the progression of the cleavage furrow, maintains the structure of the midbody, facilitates the successful abscission in the late stages of cytokinesis, and also has important functions in the early stages of mitosis and the control of DNA damage [24, 25]. KIF14 is a mitosis-related motor protein necessary for the proper positioning of the spindle during mitosis. This molecule has an important role in cytokinesis, cell division, proliferation and apoptosis. During cytokinesis, KIF14 regulates cell cycle progression and cell division by interacting with PRC1 and CIT, thereby regulating cell growth [23]. KIF4A is a motor protein localized along the axis of the chromosomes functions in the central spindle during mitosis, and is essential for the correct segregation of chromosomes [26]. TUBB3 plays a key role in the stability of the midbody microtubules, and CITK controls the stability of the midbody microtubules during cell division by regulating the phosphorylation of TUBB3. These proteins are interdependent during cytokinesis to achieve proper positioning and thus complete mitosis. Mitosis is key to the proliferation and repair of tissues or organs, and errors in the cell division process can lead to various human diseases [27]. Research has shown that the knockout of the CIT gene leads to the accumulation of DNA damage in the dorsal and ventral oligodendrocyte progenitor cells of the mouse brain, resulting in the death of the dorsal cell subpopulation and senescence of the ventral cell subpopulation, resulting in delayed growth, a shortened lifespan, ataxia, and defects in neurogenesis [25, 28, 29].

In humans, the downregulation of CIT mutations can lead to primary microcephaly [30]. CIT regulates the formation of the actin-myosin ring in cardiomyocytes. CIT is expressed at low levels in normal adult hearts, and its overexpression promotes cardiomyocyte division, leading to myocardial hypertrophy [31]. It can be inferred that the inner myometrium plays an important role in regeneration of the endometrium. After endometrial injury, the low expression of KIF14 inhibits the function of CIT, affecting the positioning of the spindle during cell division, thereby affecting the mitotic activity of endometrial cells, inhibiting the repair of the endometrium, and leading to the occurrence of IUAs.

The complement and coagulation cascade systems are key mediators of the inflammatory response following trauma, with trauma leading to the early activation of both the complement and coagulation cascades. These systems have been described as descendants of a common ancestral pathway, with both proteolytic cascades composed of serine proteases that share structural features and activate a complex network of inflammation upon tissue injury. These reactions are protective in cases of mild to moderate tissue damage but can lead to tissue injury in cases of severe trauma [32].

Upon tissue damage, the complement system, which includes more than 50 proteins, is activated through the classical, lectin, and alternative pathways to combat pathogens and clear apoptotic cells [33]. Compared with those in normal uterine myometrium, the complement components CFI, C3, C4A, C6, and C7 were downregulated in IUAs lesional tissue. CFI is essential for complement regulation [34]. CFI deficiency can result in vasculitis due to failed immune complex clearance, triggering inflammation and neutrophil chemotaxis [35–37]. C3, which is central to innate immunity, may disrupt iron metabolism and immune function when it is deficient [38]. C4, which is crucial for pathogen recognition, generates fragments with anti-inflammatory effects. Its deficiency can impair complement activation and phagocytic cell function [39]. C4A downregulation may affect endothelial function [40]. C6, part of the membrane attack complex (MAC), contributes to cell lysis and immune clearance [41]. C7, which is part of the terminal complement complex, may affect complement activation and interact with the coagulation system, contributing to tissue damage [42]. This finding offers theoretical evidence that stem cells may alleviate IUAs via immune modulation [43]. Thus, severe endometrial injury may trigger excessive complement system activation and component depletion. On the one hand, this effect may lead to impaired clearance of immune complexes and their deposition at the site of trauma, causing the accumulation of inflammatory cytokines leading to the formation of adhesions, affecting

the normal repair of the endometrium, and increasing the risk of infection. On the other hand, a deficiency in complement components may lead to vascular endothelial dysfunction, reducing the blood supply and nutrient transport to the site of injury, thereby affecting the repair of the endometrium.

The activation of the coagulation cascade is a crucial response to trauma, preventing bleeding. However, severe injury can lead to a deficiency in coagulation-related substances [32]. In this study, the levels of the procoagulation substances clusterin (CLU), HCII, and vitamin K-dependent protein S were significantly lower in the S group than in Group I. CLU is involved in DNA repair, protein homeostasis, and cell survival signaling, and is implicated in apoptosis, cell adhesion, tissue remodelling, and lipid transport [44]. CLU expression is negatively correlated with liver fibrosis and is downregulated in paediatric nonalcoholic fatty liver disease (NAFLD) patients compared with that in healthy children [45, 46]. In biliary atresia (BA), post-Kasai portoenterostomy CLU levels are negatively correlated with liver damage and fibrosis [5]. CLU gene knockout mice show exacerbated liver fibrosis after carbon tetrachloride injection, whereas CLU overexpression ameliorates liver fibrosis, possibly by inhibiting hepatic stellate cell activation and Smad3 signalling [47]. CLU expression is weaker in fibrotic lung tissue than in normal tissue, and TGF- $\beta$ 1 decreases CLU expression in fibroblasts, suggesting its role in limiting uncontrolled fibroblast proliferation [48]. Importantly, CLU is also expressed in normal endometrial tissue [49, 50]. Furthermore, HCII, a plasma protease inhibitor, has potential anti-liver fibrosis effects, with activity that is negatively correlated with liver fibrosis in NAFLD and T2DM patients [47]. In brief, it is hypothesized that endometrial injury and the downregulation of procoagulant substances such as CLU and HCII may contribute to endometrial fibrosis in IUAs patients.

The ECM-receptor interaction can regulate cellular processes for repair after injury. In this study, KEGG analysis identified two key proteins in the ECM-receptor interaction pathway. The first is TSP-4, which is downregulated in both Groups S and M, and is crucial for angiogenesis under stress [51, 52]. The overexpression of this molecule in bone marrow mesenchymal stem cells promotes angiogenesis in ischaemia models [53]. Another protein is platelet glycoprotein 4, which is upregulated only in Group S, and is a receptor for TSP-1 and TSP-2, which have contrasting effects on TSP-4 and are profibrotic [54–56]. In addition, since the ECM is composed of various collagen proteins, excessive deposition of ECM might promote endometrial fibrosis and formation. In this study, compared with those in Group I, the upregulation of integrins (ITGAL, ITGAX, ITGA2B,

and ITGA4), as well as the downregulation of matrix metalloproteinases inhibitors (TIMP1 and TIMP3), was observed only in Group M and not in Group S. Integrins activate matrix metalloproteinases (MMPs) through interactions with the ECM, subsequently participating in ECM degradation. Consistently, decreased TIMP1 and TIMP3 also promote ECM degradation [57]. This result is consistent with the findings of Zi-Ang Fang et al. [21]. Thus, it is hypothesized that in mild to moderate endometrial injury, decreased TSP-4 and increased integrins promote repair through angiogenesis and ECM breakdown. In severe injury, increased platelet glycoprotein 4 and disrupted integrin signalling inhibit these processes, resulting in failed repair and adhesion.

### Limitations and perspectives

This study has many limitations. First, the sample size was small because of the strict inclusion and exclusion criteria, as well as the limited study period. Second, the significant biomarkers and correlated signalling pathways were identified mainly through bioinformatic analyses, and they were not validated with other technologies to make the results more convincing. Additionally, the study lacked normal endometrial tissue as a control, which affected the exploration of the pathogenesis of IUAs to some extent. Therefore, in the future, we plan to expand the sample size and study duration, as well as add a normal endometrium as a control. For several key biomarkers, such as CIT and KIF14, in addition to tissue-level molecular experiments such as Western blot and qPCR, we plan to develop a uterine organoid gene knockdown model using viral transfection. This model will be transplanted into IUAs animal models to delve into the reparative mechanisms of uterine organoids. Finally, the identified genes will undergo gene editing in uterine organoids derived from patients, and these organoids will be retransplanted into the patient's uterine cavity, thereby achieving precise, individualized clinical treatment for IUAs.

### Conclusions

In summary, through transcriptomic and proteomic technology, this study revealed the correlation of endometrial injury with the myometrium. These findings preliminarily revealed that the myometrium possibly contributes to the aetiology and progression of IUA through dual mechanisms. On the one hand, the myometrium inhibits endometrial regeneration by suppressing the cell mitogenic pathway. On the other hand, it promotes fibrosis by activating the complement-coagulation cascade system and inhibiting the ECM degradation pathway. These new findings increase our understanding of the pathogenesis of IUAs and potentially contribute to the application of precision clinical treatment for IUAs.

### Acknowledgements

The authors would like to thank all members of the Department of Gynaecology at the Second Hospital of Hebei Medical University for their scientific advice and encouragement.

### Authors' contributions

X. X. and K. G. were in charge of conceptualization, methodology, data curation, formal analysis, and writing draft. P. Z. charged of resources, methodology, data curation and formal analysis. X. Z. charged of resources, methodology and formal analysis. P.Z. charged of resources and methodology. X.S. and M. Z. charged of resources. Y. T. and L.F. charged of data curation. X. H. and J. Z. charged of conceptualization, funding acquisition, and supervision. All authors reviewed the manuscript.

### Funding

This work was supported by the Hebei Provincial Health Commission Medical Science Research Project (No.20240734), the Central Government Guided Local Science and Technology Development Fund Project (Science and Technology Innovation Base Project) (No.236Z7756G), Provincial Natural Science Foundation of Hebei (No.H2024206433) and Henan Medical Science and Technology Research Program (grant no. LHGJ20220359).

### Data availability

The datasets generated and/or analysed during the current study are available in the GSA repository, <https://ngdc.cncb.ac.cn/gsa-human/s/004lqX3E>.

### Declarations

#### Ethics approval and consent to participate

This study was conducted with the approval of the Ethics Committee of the Second Hospital of Hebei Medical University. It was conducted in accordance with the ethical standards of the World Medical Association's Declaration of Helsinki, which provides guidance on the ethical considerations for medical research involving human subjects. Informed consent was obtained from all individual participants included in the study.

#### Consent for publication

Not applicable.

#### Competing interest

The authors declare no competing interests.

#### Author details

<sup>1</sup>Department of Gynecology, The Second Hospital of Hebei Medical University, 215 Peace Road West, Shijiazhuang 050000, Hebei, China. <sup>2</sup>Hebei Key Laboratory of Regenerative Medicine of Obstetrics and Gynecology, Shijiazhuang 050000, Hebei, China. <sup>3</sup>Department of Nephrology, The Second Affiliated Hospital of Xi'an Jiaotong University, Xi'an, Shaanxi 710004, China. <sup>4</sup>Department of Pelvic Floor Clinic, Cangzhou Central Hospital, Cangzhou 061000, Hebei, China. <sup>5</sup>Department of Reproductive Medicine, The Second Hospital of Hebei Medical University, Shijiazhuang 050000, Hebei, China. <sup>6</sup>Department of Gynecology, The First Affiliated Hospital of Zhengzhou University, Zhengzhou 450052, Henan, China. <sup>7</sup>Department of Gynecology, The Fourth Hospital of Shijiazhuang, Shijiazhuang 050011, Hebei, China.

Received: 10 October 2024 Accepted: 7 March 2025

Published online: 11 April 2025

### References

1. Healy MWH, Schexnayder B, Connell MT, Terry N, DeCherney AH, Csokmay JM, Yauger BJ, Hill MJ. Intrauterine adhesion prevention after hysteroscopy: a systematic review and meta-analysis. *Am J Obstet Gynecol*. 2016;214(5):576–587.e4.
2. Prianishnikov VA. On the concept of stem cell and a model of functional-morphological structure of the endometrium [J]. *Contraception*. 1978;18(3):213–23.
3. Vitale SG, Riemma G, Ciebiera M, Cianci S. Hysteroscopic treatment of submucosal fibroids in perimenopausal women: when, why, and how?

- Climacteric. 2020;23(4):355–9. <https://doi.org/10.1080/13697137.2020.1754390>.
4. Hooker AB, Lemmers M, Thurkow AL, Heymans MW, Opmeer BC, Broëlmann HAM, Mol BW, Huirne JAF. Systematic review and meta-analysis of intrauterine adhesions after miscarriage: prevalence, risk factors and long-term reproductive outcome. *Hum Reprod Update*. 2014;20(2):262–78. <https://doi.org/10.1093/humupd/dmt045>.
  5. Lee W-L, Liu C-H, Cheng M, Chang W-H, Liu W-M, Wang P-H. Focus on the Primary Prevention of Intrauterine Adhesions: Current Concept and Vision. *Int J Mol Sci*. 2021;22(10):5175. <https://doi.org/10.3390/ijms22105175>.
  6. Khan Z, Goldberg JM. Hysteroscopic management of asherman's syndrome: special issue report on uterine surgery in the journal of minimally invasive gynecology. *J Minim Invasive Gynecol*. 2017. <https://doi.org/10.1016/j.jmig.2017.09.020>.
  7. Vitale SG, Riemma G, Carugno J, et al. Postsurgical barrier strategies to avoid the recurrence of intrauterine adhesion formation after hysteroscopic adhesiolysis: a network meta-analysis of randomized controlled trials. *Am J Obstet Gynecol*. 2021. <https://doi.org/10.1016/j.ajog.2021.09.015>.
  8. Munro MG, Abbott JA, Bradley LD, et al. AAGL Practice Report: practice guidelines on intrauterine adhesions developed in collaboration with the european society of gynaecological endoscopy (ESGE). *J Minim Invasive Gynecol*. 2017. <https://doi.org/10.1016/j.jmig.2016.11.008>.
  9. Zhou Q, Shi X, Saravelos S, Huang X, Zhao Y, Huang R, Xia E, Li T. Auto-Cross-Linked hyaluronic acid gel for prevention of intrauterine adhesions after hysteroscopic adhesiolysis: a randomized controlled trial. *J Minim Invasive Gynecol*. 2020. <https://doi.org/10.1016/j.jmig.2020.06.030>.
  10. Guo Y, Shi X, Song D, Liu Y, Huang X, Xiao Y, Yang L, Xia E, Li T-C. The efficacy of auto-cross-linked hyaluronic acid gel in addition to oestradiol and intrauterine balloon insertion in the prevention of adhesion reformation after hysteroscopic adhesiolysis. *RBMO*. 2022;00:1–7. <https://doi.org/10.1016/j.rbmo.2022.04.017>.
  11. Zheng JH, Zhang JK, Kong DS, et al. Quantification of the CM-Dil-labeled human umbilical cord mesenchymal stem cells migrated to the dual injured uterus in SD rat [J]. *Stem Cell Res Ther*. 2020;11(1):280.
  12. Li W, Gu P, Gao B, et al. Characteristics and transcriptomic analysis of scar tissues on the inner uterine cavity wall in patients with intrauterine adhesions [J]. *Fron Physiol*. 2022;13:990009.
  13. Mehasseb MK, Taylor AH, Pringle JH, et al. Enhanced invasion of stromal cells from adenomyosis in a three-dimensional coculture model is augmented by the presence of myocytes from affected uteri [J]. *Fertil Steril*. 2010;94(7):2547–51.
  14. Brosens I, Pijnenborg R, Benagiano G. Defective myometrial spiral artery remodelling as a cause of major obstetrical syndromes in endometriosis and adenomyosis. *Placenta*. 2013;34(2):100–5. <https://doi.org/10.1016/j.placenta.2012.11.017>.
  15. Harmsen MJ, Trommelen LM, de Leeuw RA, et al. Uterine junctional zone and adenomyosis: comparison of MRI, transvaginal ultrasound and histology [J]. *Ultrasound Obstet Gynecol*. 2023;62(1):42–60.
  16. Hunt S, Abdallah KS, Ng E, et al. Impairment of Uterine Contractility Is Associated with Unexplained Infertility [J]. *Seminars in Reproductive Medicine*. 2020;38(01):061–73.
  17. Kang K, Wang A, Wu H. Magnetic Resonance Imaging for Diagnosing Intrauterine Adhesions. *J Obstet Gynaecol Can*. 2023. <https://doi.org/10.1016/j.jogc.2023.06.004>.
  18. He J, Jia Y. Application of omics technologies in dermatological research and skin management [J]. *J Cosmet Dermatol*. 2021;21(2):451–60.
  19. Fredman G, Skov L, Mann M, et al. Towards Precision Dermatology: Emerging Role of Proteomic Analysis of the Skin [J]. *Dermatology*. 2022;238(2):185–94.
  20. Xu C, Bao M, Fan X, Huang J, Zhu C, Xia W. EndMT: New findings on the origin of myofibroblasts in endometrial fibrosis of intrauterine adhesions. *Reprod Biol Endocrinol*. 2022;20:9. <https://doi.org/10.1186/s12958-022-00887-5>.
  21. Fang Z-A, He Y, Sun C, Zhan L, Zhou G, Wei B, Sun S. Expression and potential role of CXCL5 in the pathogenesis of intrauterine adhesions. *J Int Med Res*. 2021;49(3):1–15. <https://doi.org/10.1177/0300060521997718>.
  22. Liu D, Yuan L, Xu F, Ma Y, Zhang H, Jin Y, Chen M, Zhang Z, Luo S. Interleukin-33 promotes intrauterine adhesion formation in mice through the mitogen-activated protein kinase signaling pathway. *Commun Biol*. 2024;7:1022. <https://doi.org/10.1038/s42003-024-06709-1>.
  23. Gruneberg U, Neef RD, Li X, et al. KIF14 and citron kinase act together to promote efficient cytokinesis [J]. *J Cell Biol*. 2006;172(3):363–72.
  24. Maw JJ, Coker JA, Arya T, et al. Discovery and Characterization of Selective, First-in-Class Inhibitors of Citron Kinase [J]. *J Med Chem*. 2024;67(4):2631–66.
  25. D'Avino PP. Citron kinase – renaissance of a neglected mitotic kinase [J]. *J Cell Sci*. 2017;130(10):1701–8.
  26. Poser E, Caous R, Gruneberg U, et al. Aurora A promotes chromosome compression by activating the condensin-dependent pool of KIF4A [J]. *J Cell Biol*. 2019;219(2):e201905194.
  27. Sgrò F, Bianchi FT, Falcone M, et al. Tissue-specific control of midbody microtubule stability by Citron kinase through modulation of TUBB3 phosphorylation [J]. *Cell DeathDif*. 2015;23(5):801–13.
  28. Boda E, Lorenzati M, Parolisi R, et al. Molecular and functional heterogeneity in dorsal and ventral oligodendrocyte progenitor cells of the mouse forebrain in response to DNA damage [J]. *Nat Commun*. 2022;13(1):2331.
  29. di Cunto F, Imarisio S, Hirsch E, et al. Defective neurogenesis in citron kinase knockout mice by altered cytokinesis and massive apoptosis [J]. *Neuron*. 2000;28(1):115–27.
  30. Moawia A, Shaheen R, Rasool S, et al. Mutations of KIF14 cause primary microcephaly by impairing cytokinesis [J]. *Ann Neurol*. 2017;82(4):562–77.
  31. Ahuja P, Perriard E, Pedrazzini T, et al. Re-expression of proteins involved in cytokinesis during cardiac hypertrophy [J]. *Exp Cell Res*. 2007;313(6):1270–83.
  32. Satyam A, Graef ER, Lapchak PH, et al. Complement and coagulation cascades in trauma [J]. *Acute Medicine & Surgery*. 2019;6(4):329–35.
  33. Pape HC, Moore EE, McKinley T, et al. Pathophysiology in patients with polytrauma [J]. *Injury*. 2022;53(7):2400–12.
  34. Hallam TM, Sharp SJ, Andreadi A, et al. Complement factor I: Regulatory nexus, driver of immunopathology, and therapeutic [J]. *Immunobiol*. 2023;228(5):152410.
  35. Zhang Y, Goodfellow RX, Ghiringhelli Borsa N, et al. Complement Factor I Variants in Complement-Mediated Renal Diseases [J]. *Frontiers in Immunol*. 2022;13:866330.
  36. Rakhola D, Lipitsa T, Siiskonen H, et al. Sequential Increase in Complement Factor I, iC3b, and Cells Expressing CD11b or CD14 in Cutaneous Vasculitis [J]. *Analyt Cell Pathol*. 2022;2022:3888734.
  37. Levit E, Leon J, Lincoln MR. Pearls & Oysters: homozygous complement factor I deficiency presenting as fulminant relapsing complement-mediated CNS vasculitis [J]. *Neurol*. 2023;101(2):e220–e3.
  38. Wang Q, Rozelle AL, Lepus CM, et al. Identification of a central role for complement in osteoarthritis [J]. *Nat Med*. 2011;17(12):1674–9.
  39. Wang H, Liu M. Complement C4, Infections, and Autoimmune Diseases [J]. *Front Immunol*. 2021;12:694928.
  40. Xue L, Xie K, Wu L, et al. A novel peptide relieves endothelial cell dysfunction in preeclampsia by regulating the PI3K/mTOR/HIF1 $\alpha$  pathway [J]. *Int J Mol Med*. 2020;47(1):276–88.
  41. Ricklin D, Hajishengallis G, Yang K, et al. Complement: a key system for immune surveillance and homeostasis [J]. *Nat Immunol*. 2010;11(9):785–97.
  42. Cervia-hasler C, Brüningk SC, Hoch T, et al. Persistent complement dysregulation with signs of thromboinflammation in active Long Covid [J]. *Sci*. 2024;383(6680):eadg7942.
  43. Chen J-m, Huang Q-y, Zhao Y-x, Chen W-h, Lin S, Shi Q-y. The latest developments in immunomodulation of mesenchymal stem cells in the treatment of intrauterine adhesions, both allogeneic and autologous. *Front Immunol*. 2021;12:785717. <https://doi.org/10.3389/fimmu.2021.785717>.
  44. Zhang Q, Yue Y, Zheng R. Clusterin as a serum biomarker candidate contributes to the lung fibroblasts activation in chronic obstructive pulmonary disease [J]. *Chin Med J*. 2022;135(9):1076–86.
  45. Udomsinprasert W, Poovorawan Y, Chongsrisawat V, et al. Decreased circulating clusterin reflects severe liver complications after hepatoporoenterostomy of biliary atresia [J]. *Sci Rep*. 2020;10(1):19736.
  46. Małcki P, Tracz J, Łuczak M, et al. Serum proteome assessment in nonalcoholic fatty liver disease in children: a preliminary study [J]. *Expert Rev Proteomics*. 2020;17(7–8):623–32.
  47. Seo HY, Lee SH, Lee JH, et al. Clusterin attenuates hepatic fibrosis by inhibiting hepatic stellate cell activation and downregulating the smad3 signaling pathway [J]. *Cells*. 2019;8(11):1442.
  48. Peix L, Evans IC, Pearce DR et al. Diverse functions of clusterin promote and protect against the development of pulmonary fibrosis [J]. *Sci Rep*. 2018;8(1):1906.

49. Fuzio P, Valletti A, Napoli A, et al. Regulation of the expression of CLU isoforms in endometrial proliferative diseases [J]. *Int J Oncol*. 2013;42(6):1929–44.
50. Konrad L, Hackethal A, Oehmke F, et al. Analysis of Clusterin and Clusterin Receptors in the Endometrium and Clusterin Levels in Cervical Mucus of Endometriosis [J]. *Reprod Sci*. 2016;23(10):1371–80.
51. Stenina-adognravi O, Plow EF. Thrombospondin-4 in tissue remodeling [J]. *Matr Biol*. 2019;75–76:300–13.
52. Genaro K, Luo ZD. Pathophysiological roles of thrombospondin-4 in disease development [J]. *Semin Cell Dev Biol*. 2024;155(Pt B):66–73.
53. Ge HA, Shrestha A, Liu C, et al. MicroRNA 148a–3p promotes Thrombospondin-4 expression and enhances angiogenesis during tendinopathy development by inhibiting Krüppel-like factor 6 [J]. *Biochem Biophys Res Commun*. 2018;502(2):276–82.
54. Matilla L, Martín-núñez E, Garaikoetxea M, et al. Characterization of the sex-specific pattern of angiogenesis and lymphangiogenesis in aortic stenosis [J]. *Front Cardiovasc Med*. 2022;9:971802.
55. Liao X, Yan S, Li J, et al. CD36 and Its Role in Regulating the Tumor Micro-environment [J]. *Curr Oncol*. 2022;29(11):8133–45.
56. Lawler PR, Lawler J. Molecular basis for the regulation of angiogenesis by thrombospondin-1 and -2 [J]. *Cold Spring Harbor Perspect in Med*. 2012;2(5):a006627-a.
57. Park EJ, Myint PK, Ito A, et al. Integrin-Ligand Interactions in Inflammation, Cancer, and Metabolic Disease: Insights Into the Multifaceted Roles of an Emerging Ligand Irisin [J]. *Front Cell Develop Biol*. 2020;8.

### **Publisher's Note**

Springer Nature remains neutral with regard to jurisdictional claims in published maps and institutional affiliations.